by thermodynamic arguments: the greater flexibility of AT vs GC regions, the steric effects of the guanine amino group, the differences in potential in the GC and AT regions, etc. Alternatively, the apparent intercalative binding of TMpyP(4) and group I metalloporphyrins contrasted with the absence of such binding by group III porphyrins is explained by either a thermodynamic/steric argument (the presence of axial ligands) or a kinetic/steric argument (inability to achieve a planar structure for TMpyP(2), etc).

As stated above, our major objectives here involved evaluating the effects of metalloporphyrins on DNA properties to identify areas where fruitful studies might be conducted with oligonucleotides. However, the apparent differences in effects of group I porphyrins (TMpyP(4), NiTMpyP(4), and PdTMpyP(4)) when combined with the selectivity of TMpyP(4) for 5'-CG-3' over 5'-GC-3' sites have led us to wonder if all effects are not best explained by primarily a thermodynamic/steric argument. The highly charged porphyrins appear to be binding by many competitive modes. If such subtle differences between the group I porphyrins and between sequences lead to differences in binding, then perhaps major changes (TMpyP(4) to TMpyP(2), *N*-methylpyridiniumyl to trimethylaniliniumyl) could make intercalative binding unfavorable. (Again, we repeat that we do not claim that intercalative binding has been established beyond question). For example, steric effects of the *N*-methyl groups of TMpyP(2) could easily prevent intercalation from being thermodynamically possible. Likewise, intercalated TMAP, with its positive groups ca. 1.5 Å further out from the porphyrin center than TMpyP(4), might not be able to form as favorable interactions with the phosphate groups of DNA as does intercalated TMpyP(4).

We believe that this thermodynamic/steric model explains the interaction of complex molecules, like the porphyrins, with DNA and offers an alternative to the "temporarily planar" kinetic explanation for additional reasons. First, complex molecules such as nogalamycin[52,53] and naphthalenediimides,[54,55] which have bulky groups on opposite sides of the planar ring system and which cannot become planar, bind to DNA by intercalation. Second, model building studies indicated that porphyrins, even with the pyridyl groups in the plane of the porphyrin ring, still require significant disruption of the double helix to allow intercalation.

It is clear that a complete understanding of the factors influencing binding of these intriguing porphyrin species must await further information on binding modes and additional kinetic measurements. In particular, studies with oligonucleotides may allow us to differentiate between the models. Oligonucleotides undergo large amplitude dynamic motions, including complete strand separation. These motions would easily allow TMpyP(2) to intercalate if only a kinetic barrier prevented insertion of the porphyrin.

Acknowledgment. This work was supported by NIH Grant GM 29222 to L.G.M. and NSF Grant DBM 8603566 to W.D.W. The Col E_1 CCS DNA was a gift from Dr. Robert L. Jones. The 360-MHz NMR spectrometer was purchased with partial support from the NSF through a departmental grant to Emory University.

(52) Arora, S. K. *J. Am. Chem. Soc.* **1983**, *105*, 1328.
(53) Collier, D. A.; Neidles, S.; Brown, J. R. *Biochem. Pharmacol.* **1984**, *33*, 2877.
(54) Yen, S. F.; Gabbay, E. J.; Wilson, W. D. *Biochemistry* **1982**, *21*, 2070.
(55) Hopkins, H. P.; Stevenson, K. A.; Wilson, W. D. *J. Solution Chem.* **1986**, *15*, 563.

Notes

Contribution from the Dipartimento di Chimica Inorganica, Metallorganica ed Analitica, Università di Padova, Padova, Italy, Istituto di Chimica e Tecnologia dei Radioelementi del CNR, Padova, Italy, and Dipartimento di Chimica Inorganica e Struttura Molecolare, Università di Messina, Messina, Italy

UV Photoelectron Spectra and DV-Xα Calculations on Rh_2^{4+} Formamidinate Complexes

Gian Andrea Rizzi,[1a] Maurizio Casarin,[1b] Eugenio Tondello,[1a] Pasquale Piraino,[1c] and Gaetano Granozzi*[1a]

Received March 2, 1987

Complexes containing the Rh_2^{4+} core have been extensively investigated from both the synthetic[2] and spectroscopic[2] points of view, and their possible applications have been outlined.[3] Most of these studies have been directed toward complexes containing four carboxylate groups as bridging ligands.

Several theoretical studies (using both MS-Xα and minimal basis-set ab initio methods) on the nature of the Rh-Rh bond in carboxylates have been reported.[4] They are all in agreement with the existence of a single Rh-Rh bond, but different electronic configurations for the tetraformate $Rh_2[O_2CH]_4$ complex (**1**) have been obtained according to the different theoretical approaches (MS-Xα,[4a] $\sigma^2\pi^4\delta^2\pi^{*4}\delta^{*2}$; ab initio,[4b] $\pi^4\delta^2\pi^{*4}\delta^{*2}\sigma^2$). However, no experimental determination of one-electron levels by gas-phase photoelectron (PE) spectroscopy has been reported so far because of the thermal decomposition of the carboxylate dimers in the ionization chamber. To our knowledge, the unique PE literature data regarding Rh_2^{4+} complexes refer to the complex $Rh_2(mhp)_4$ (mhp = 2-oxo-6-methylpyridinate), where a $\sigma^2\pi^4\delta^2\pi^{*4}\delta^{*2}$ configuration was proposed in order to nicely fit the experimental data.[5]

Recently, complexes containing formamidinate ligands have been prepared and structurally characterized[6] and the attempt to record their PE spectra has been successful. In this contribution we report the UV excited PE spectra of $Rh_2[HC(NR)_2]_2[O_2CCF_3]_2$ (**2**) and $Rh_2[HC(NR)_2]_4$ (**3**) (R = *p*-tolyl) coupled with the results of *first-principle* discrete variational (DV) Xα quantum-mechanical calculations[7] carried out on the $Rh_2[HC(NH)_2]_2[O_2CH]_2$ (**2a**) and $Rh_2[HC(NH)_2]_4$ (**3a**) models.

Experimental Section

Synthesis. The samples of $Rh_2[HC(NR)_2]_2[O_2CCF_3]_2(H_2O)_2$ (**2c**) and $Rh_2[HC(NR)_2]_4$ (**3**) (R = *p*-tolyl) were synthesized according to the published procedures.[6] After crystallization, their purity was checked by IR and NMR measurements.

(1) (a) University of Padova. (b) CNR of Padova. (c) University of Messina.
(2) (a) Boyar, E. B.; Robinson, S. D. *Coord. Chem. Rev.* **1983**, *50*, 109. (b) Felthouse, T. R. *Prog. Inorg. Chem.* **1982**, *29*, 73.
(3) (a) Hughes, R. G.; Bear, J. L.; Kimball, A. P. *Proc. Am. Assoc. Cancer Res.* **1972**, *13*, 120. (b) Howard, R. A.; Kimball, A. P.; Bear, J. L. *Cancer Res.* **1979**, *39*, 2568.
(4) (a) Norman, J. G., Jr.; Kolari, H. J. *J. Am. Chem. Soc.* **1979**, *101*, 5256. (b) Nakatsuji, H.; Ushio, T.; Kanda, K.; Onishi, Y.; Kawamura, T.; Yonezawa, T. *Chem. Phys. Lett.* **1981**, *79*, 299.
(5) Berry, M.; Garner, C. D.; Hillier, I. H.; McDowell, A. A.; Clegg, W. *J. Chem. Soc., Chem. Commun.* **1980**, 494.
(6) (a) Piraino, P.; Bruno, G.; Tresoldi, G.; Lo Schiavo, S.; Zanello, P. *Inorg. Chem.* **1987**, *26*, 91. (b) Piraino, P.; Bruno, G.; Tresoldi, G.; Lo Schiavo, S.; Zanello, P. *Inorg. Chem.*, in press.
(7) (a) Averill, F. W.; Ellis, D. E. *J. Chem. Phys.* **1973**, *59*, 6411. (b) Rosen, A.; Ellis, D. E.; Adachi, H.; Averill, F. W. *J. Chem. Phys.* **1976**, *65*, 3629 and references therein. (c) Trogler, W. C.; Ellis, D. E.; Berkowitz, J. *J. Am. Chem. Soc.* **1979**, *101*, 5896.

0020-1669/87/1326-3406$01.50/0

Table I. DV–Xα Results on $Rh_2[HC(NH)_2]_4$

MO	$-\epsilon$, eV	population, % 2 Rh s	2 Rh p	2 Rh d	8 N	4 C	12 H	dominant character[a]
$4a_{2u}$ (LUMO)	1.58	15	5	67	12		1	σ^* Rh–Rh
$2b_{1u}$ (HOMO)	2.04			62	38			δ^* Rh–Rh, π Rh–N ab
$5e_g$	3.08			95	1	1	3	π^* Rh–Rh
$1a_{1u}$	3.99				100			N nb
$2b_{2g}$	4.15			75		25		δ Rh–Rh
$4e_g$	4.63				100			N nb
$6e_u$	4.76			89	5	3	3	π Rh–Rh
$5a_{1g}$	5.30	18		72	7	1	2	σ Rh–Rh
$5e_u$	5.88		3	2	67	10	18	σ ligand
$1b_{1u}$	6.79			31	69			π Rh–N b
$3e_g$	7.05		2		92	1	5	N nb
$4a_{1g}$	7.94	4		17	49	12	18	σ Rh–N b
$1a_{2g}$	7.95				46	54		π ligand
$4b_{1g}$	8.20			37	33	14	16	σ Rh–N b
$4e_u$	8.56				52	48		π ligand

[a] Legend: b = bonding; ab = antibonding; nb = nonbonding.

Spectra. He I and He II excited PE spectra were measured on a Perkin-Elmer PS-18 spectrometer modified for He II measurements by inclusion of a hollow cathode discharge lamp giving a high output of He II photons (Helectros Developments). The ionization energy (IE) scale was calibrated by reference to peaks due to admitted inert gases (Xe–Ar) and to the He $1s^{-1}$ self-ionization. A heated inlet probe system was adopted at 290 °C (**3**) and 210 °C (**2c**). Under the experimental conditions in the ionization chamber complex **2c** loses the axial water molecules, giving rise to **2**, as clearly monitored by the presence (in the 50–70 °C temperature range) of the PE peaks due to the free H_2O molecule.

Theoretical Method. Hartree–Fock–Slater (HFS) discrete variational (DV–Xα) calculations[7] were performed on a VAX 8600 computer. Numerical atomic orbitals obtained for the neutral atoms (through 5p for Rh and 2p for C, N, and O) were used as basis functions. Due to the size of the investigated systems, orbitals 1s–4p on Rh and 1s on C, N, and O were treated as a frozen core in the molecular calculations. A self-consistent multicenter–multipolar (SCM) representation of the density is introduced according to a procedure described elsewhere.[8] Five radial degrees of freedom were allowed in the expansion of the density in addition to radial atomic densities. The Gaspar–Kohn–Sham value[9] for the exchange scaling parameter has been adopted ($\alpha = {}^2/_3$). Atomic orbital populations were computed by using the Mulliken analysis.[10] To evaluate the magnitude of electronic relaxation associated with the removal of one electron from the various ground-state MOs, IE calculations were carried out by using Slater's transition-state formalism (TSIE).[11] Calculations have been carried out on **2a** and **3a** models by using the geometrical parameters obtained from the solid-state structural determinations of **2c**[6a] and **3**[6b] and assuming perfect C_{2v} (for **2a**) and D_{4h} (for **3a**) structures (see Figure 1 for the axis convention).

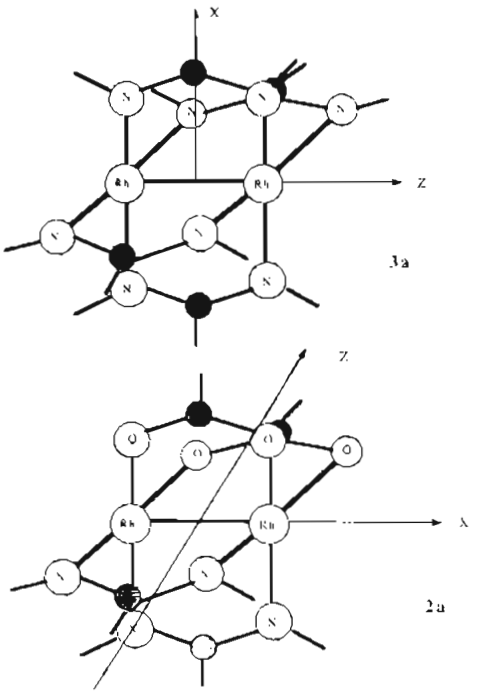

Figure 1. Schematic views of investigated molecules. The axis system is also reported.

Results and Discussion

In Table I the charge density analysis of the outermost MOs of **3a** is reported. The dominant character has been assigned on the basis of symmetry considerations and by an accurate analysis of the relative wave functions.

The electronic configuration describing the metal–metal interaction is $\sigma^2\pi^4\delta^2\pi^{*4}\delta^{*2}$. A single Rh–Rh bond is then predicted because only the σ component ($5a_{1g}$) has an empty antibonding counterpart (the $4a_{2u}$ LUMO). The population analysis shows that 5s and 5p Rh orbitals are slightly involved in the metal–metal bonding, the only significant contribution arising from the 5s orbital in the σ and σ^* MOs.

It is interesting to notice that some MOs, involved in the metal–metal interaction, have also a relevant metal–ligand, either bonding or antibonding, character (Table I). For example, both $1b_{1u}$ and $2b_{1u}$ MOs have a δ^* M–M character,[12] but the outermost one ($2b_{1u}$ HOMO) also has an antibonding Rh–N π character, while the innermost $1b_{1u}$ has a π Rh–N bonding character. Other MOs contributing to the Rh–ligand bonding are $4a_{1g}$ and $4b_{1g}$ (σ in nature). Orbitals of the e_g and e_u type do not contribute at all to the metal–ligand interaction and are localized either in the metal or in the ligand framework.

A correlation diagram between the ground-state DV–Xα levels of the formamidinate complexes **2a** and **3a** and those obtained from a similar calculation on the $Rh_2[O_2CH]_4$ tetraformate complex (**1**) is reported in Figure 2. Simple electronegativity arguments about the bridging ligands (oxygen vs. nitrogen) can explain the progressive destabilization of all the valence levels on going from **1** toward **3a**.

In all three cases the presence of a single metal–metal bond is predicted, in agreement with previous theoretical studies.[4] It is interesting to note the enhancement of the energy separation between the π^* and δ^* components on going from **1** toward **3a**. This effect can be easily explained by taking into account the

(8) Delley, B.; Ellis, D. E. *J. Chem. Phys.* **1982**, *76*, 1949.
(9) (a) Gaspar, R. *Acta Phys. Acad. Sci. Hung.* **1954**, *3*, 263. (b) Kohn, W.; Sham, L. J. *Phys. Rev.* **1965**, *140*, A1133.
(10) Mulliken, R. S. *J. Chem. Phys.* **1955**, *23*, 1833.
(11) Slater, J. C. *Quantum Theory of Molecules and Solids. The Self-Consistent Field for Molecules and Solids*; McGraw-Hill: New York, **1974**; Vol. 4.

(12) The outermost $2b_{1u}$ MO has the largest localization on the metallic centers, and it has been taken as representative of the δ^* interaction

Table II. IE and TSIE Values (eV) of $Rh_2[HC(NR_2)]_4$ and $Rh_2[HC(NR_2)]_2[O_2CCF_3]_2$ (R = *p*-Tolyl)

$Rh_2[HC(NR_2)]_4$				$Rh_2[HC(NR_2)]_2[O_2CCF_3]_2$			
band	IE	assignt	TSIE	band	IE	assignt	TSIE
A	5.69	$2b_{1u}$	4.85	A	6.68	$10b_1$	6.48
B	6.63	$5e_g + 1a_{1u}$	6.39, 6.43	B	7.21	$8a_2$	7.98
C	7.36	$2b_{2g}$	7.06	C	7.70	$9a_2 + 9b_1$	7.41, 7.51
D	7.84	$4e_g$	7.05	D	8.37	$(13a_1 + 12a_1 + 11b_2 + 8b_1)$	8.48, 8.51, 8.50, 8.76
E	8.56	$6e_u$	7.81	E	9.12		
E′	9.43	$5a_{1g}$	8.55	E′	9.85	$11a_1$	9.58
F	11.22			F	10.63		
G	13.50			F′	11.57		
G′	14.74			G	14.00		

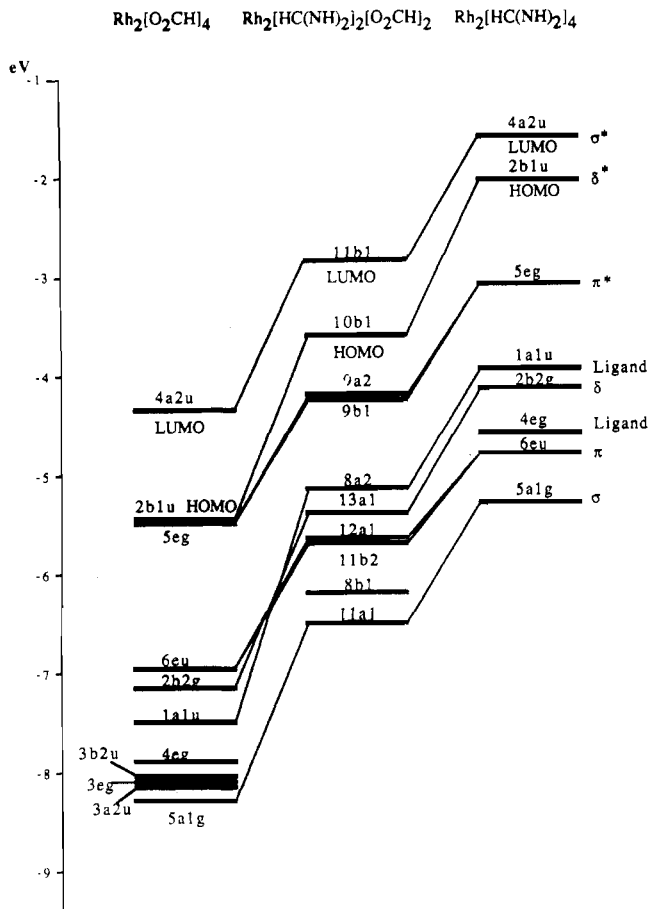

Figure 2. Correlation diagram between one-electron energy levels of **1**, **2a**, and **3a**.

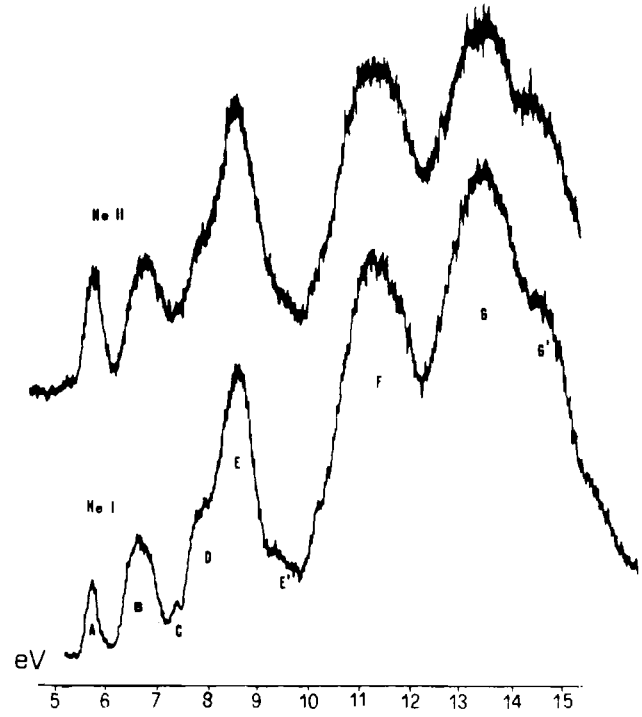

Figure 3. He I/He II excited PE spectra of $Rh_2[HC(NR)_2]_4$ (R = *p*-tolyl).

above-mentioned Rh–bridging ligand π-antibonding nature of the δ^* HOMO (see Table I): the better energy matching between the δ^* metallic orbitals and the ligand-based π orbitals, when the formamidinate ligand is considered, gives rise to a stronger Rh–ligand antibonding interaction, so destabilizing the resulting δ^* MO. Another interesting trend along the series **1** → **2a** → **3a** is the progressive destabilization of the δ component with respect to the π one, leading to a crossing between the two levels on passing from **1** to **2a** (Figure 2).

The steric hindrance due to the *p*-tolyl substituents can explain the lack of axial ligands in the crystal structure of **3**,[6b] at variance with the case for **1** and **2c**, whose crystal structures show axial water molecules.[2a,6a] However, the strong destabilization of all levels (and in particular of the $4a_{2u}$ LUMO) in the **3a** complex suggests that also an electronic factor acts adversely on the axial coordination. In fact, in a previous MS–Xα study of **1**, Norman and Kolari[4a] pointed out that the Rh–H_2O(ax) interaction is basically of σ type and arises mainly from the combination of oxygen lone pairs with the LUMO $4a_{2u}$ (σ^* Rh–Rh). Therefore, an unfavorable energy matching between the LUMO and the orbitals of the axial donor can concur to explain the scarce affinity of complex **3** toward axial ligands.

An interesting point that emerges from the calculations is that the $5e_g$ (π^* M–M) and $6e_u$ (π M–M) orbitals of **3a** (D_{4h}) are not significantly split in **2a** (by symmetry $e_g \rightarrow a_2,b_1$ and $e_u \rightarrow a_1,b_2$ in C_{2v}) so that the reduction of symmetry is only a formal matter as far as the M–M interaction is concerned. This theoretical prediction is fully confirmed by the PE spectra (see below).

The He I and He II excited PE spectra of **3** and **2** are reported in Figures 3 and 4, where bands have been alphabetically labeled. The corresponding IE values and the assignments of the lowest IE bands (the most interesting ones, since they are related to ionizations from orbitals involved in the Rh–Rh interactions) are reported in Table II. In the same table the DV–Xα-computed TSIEs are also reported. The presence of the *p*-tolyl substituents greatly complicates the PE spectra since the outermost π ionizations from the aromatic rings give rise to bands starting from ca. 8.5 eV. The assignments reported in Table II refer to ionizations from the model compounds **2a** and **3a**, with the contributions from the *p*-tolyl substituents omitted.[13,14]

According to the calculations (Tables I and II), band A of the He I PE spectrum of **3** (Figure 3) is assigned to ionization from the δ^* $2b_{1u}$ HOMO. Its relative intensity with respect to the following band B is remarkably enhanced in the He II spectrum. If we assume the usual empirical arguments about the relative

(13) For example, band E of the spectrum of **3** has been assigned to the ionization from the $6e_u$ MO (Table II) but it also contains ionizations from the aromatic rings.

(14) The CF_3 substituents only produce shifts on the outermost PE bands of the spectrum of **2** since the CF_3-localized ionizations occurr at higher IEs.

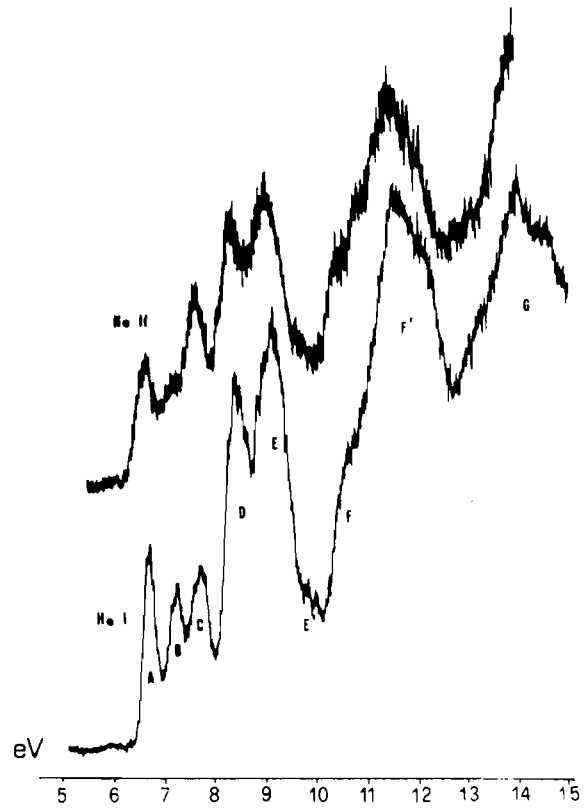

Figure 4. He I/He II excited PE spectra of $Rh_2[HC(NR)_2]_2[O_2CCF_3]_2$ (R = *p*-tolyl).

intensity variations on passing from the He I to the He II ionizing source,[15] the observed behavior can be interpreted either as a major involvement of the d metal AOs with the orbital giving rise to band A or as an indication of some component of band B arising from a ligand-localized MO. The latter hypothesis is well in tune with the theoretical results, which predict, at ca. 1.5 eV higher IE than the ionization from the HOMO, two quasi-degenerate ionizations from the $5e_g$ (π^* Rh–Rh, 95% localized on metals) and $1a_{1u}$ (100% nitrogen-based π ligand) MOs (see Table I). The presence of two components under band B is also in agreement with the splitting observed in the corresponding band of the PE spectrum of the less symmetrical complex **2** (Figure 4). The low-intensity band C (which has been confirmed by running several expanded-scale He I spectra) can be tentatively assigned to the ionization of the δ (Rh–Rh) $2b_{2g}$ MO. Its low intensity agrees well with that observed for the same ionization in the spectrum of $Rh_2(mhp)_4$.[5]

The assignments of the inner bands are complicated by the superposition of the *p*-tolyl group ionizations. We can just propose the following plausible assignments on the basis of the results of the theoretical calculations. The computed energy separations between the $4e_g$ (ligand σ/π nonbonding MO), $6e_u$ (π Rh–Rh), and $5a_{1g}$ (σ Rh–Rh) MOs lead us to ascribe their ionizations respectively to shoulder D, band E, and shoulder E′.

The He I PE spectrum of the mixed complex **2** (Figure 4) is noticeably different from that just discussed: all the bands are shifted by about 1 eV toward higher IEs, as already anticipated by our theoretical results (see Figure 2 and TSIEs in Table II). Moreover, band B of the spectrum of **3** is now split into two well-resolved components (B + C) and band D, a shoulder of band E in the previous case, is now a resolved band with an intensity comparable to that of band E. In this regard we must remember that in **2** we have only half of the aromatic rings (whose ionizations contribute to band E) that were present in the tetraformamidinate complex **3**. Very important experimental evidence is related to the change of the relative intensity between bands B and C on passing to the He II spectrum (Figure 4): the large falloff of intensity of band B is diagnostic of localization on the ligand of the corresponding MO.[15]

As in the previous case, band A is safely assigned to ionization from the $10b_1$ (δ^*) HOMO on the basis of the calculations. The assignment of bands B and C, however, needs some discussion. We have already pointed out that the symmetry reduction on passing from **3** to **2** does not produce significant energy separation on the π type metal–metal orbitals (see Figure 2 and TSIEs in Table II). According to the TSIE values obtained for the model **2a**, we should assign band B to the π^* (Rh–Rh) ($9a_2$,$9b_1$) MOs (over 90% localization on the metals) and band C to the ligand-based $8a_2$ MO (over 95% on the formamidinate ligand). This assignment, however, is in contrast with two experimentl observations: (i) band B is less intense than band C in the He I spectrum; (ii) the already mentioned decrease of the relative intensity of B vs. that of C on passing to the He II spectrum. Both these points give support to the opposite assignment, i.e. band B to $8a_2$ and band C to $9a_2$ and $9b_1$ MOs. This failure of the theoretical prediction could be ascribed to the neglect of the CF_3 groups in the model adopted for the calculations.[17]

We take band D to represent the ionizations of four MOs, namely $13a_1$ (δ bonding Rh–Rh), $12a_1$ and $12b_2$ (π bonding Rh–Rh), and $8b_1$ (localized to an equal extent on both formamidinate and carboxylate ligands). Finally, in analogy with the assignment of **3**, we propose the assignment of the $11a_1$ (σ bonding Rh–Rh) MO to the weak shoulder E′.

In conclusion, we want to stress here that the present analysis of the UV-PE data on Rh_2^{4+} formamidinate complexes furnishes an electronic configuration ($\sigma^2\pi^4\delta^2\pi^{*4}\delta^{*2}$) identical with that obtained by a previous UV-PE study on the quite different $Rh_2(mhp)_4$ complex.[5] On the other hand, all the available Xα type theoretical results[4a] (the most rigorous treatment for such complicated molecules to date) are in agreement in predicting similar configurations in both carboxylate and formamidinate complexes. We could suggest, then, that this bonding scheme can be considered as peculiar to the Rh_2^{4+} arrangement.

Acknowledgment. Financial support for this study from the Ministero della Pubblica Istruzione (Rome) is gratefully acknowledged.

Registry No. **2**, 109976-30-9; **3**, 108149-48-0.

(15) In fact, on the basis of the Gelius model for the molecular photoionization cross sections,[16] we expect a marked decrease in relative intensity for those bands containing ligand-localized ionizations with respect to metal *n*d-based ones on passing from the He I to the He II excitation source.

(16) Gelius, U. In *Electron Spectroscopy*; Shirley, D. A., Ed.; North-Holland: Amsterdam, 1972; p 311.

(17) Actually, when one deals with a less symmetrical molecule, such as **2**, the errors induced by adopting a simplified model may not be balanced. In this case, the $9a_2$ and $9b_1$ MOs have a larger localization on the carboxylate ligands than the $8a_2$ MO, so that the neglect of the large electron-withdrawing effect of the CF_3 substituents produces a shift toward lower IEs of the $9a_2$ and $9b_1$ MOs.

Contribution from the Department of Chemistry and Biochemistry, University of California, Los Angeles, California 90024-1569

Synthesis and Molecular Structures of *closo*-3-(η^6-$CH_3C_6H_5$)-3,1,2-$FeC_2B_9H_{11}$ and *closo*-3-(η^6-1,4-$(CH_3)_2C_6H_4$)-3,1,2-$FeC_2B_9H_{11}$

Han Chyul Kang, Carolyn B. Knobler, and M. Frederick Hawthorne*

Received April 16, 1987

The chemistry of mixed-sandwich transition-metal complexes of the type [(η^6-arene)M(η^5-Cp)] has been well documented in literature.[1] In view of the close structural and electronic similarity

